Rock Islands

Chapter 10
Palau

The contributions of Maria Ngemaes, Godwin Sisior and Dirutelchii Ngirengkoi from the Palau National Weather Service Office are gratefully acknowledged

Introduction

This chapter provides a brief description of Palau, its past and present climate as well as projections for the future. The climate observation network and the availability of atmospheric and oceanic data records are outlined. The annual mean climate, seasonal cycles and the influences of large-scale climate features such as the West Pacific Monsoon and patterns of climate variability (e.g. the El Niño-Southern Oscillation) are analysed and discussed. Observed trends and analysis of air temperature, rainfall, extreme events (including tropical cyclones), sea-surface temperature, ocean acidification, mean and extreme sea levels are presented. Projections for air and sea-surface temperature, rainfall, sea level, ocean acidification and extreme events for the 21st century are provided. These projections are presented along with confidence levels based on expert judgement by Pacific Climate Change Science Program (PCCSP) scientists. The chapter concludes with a summary table of projections (Table 10.3). Important background information including an explanation of methods and models is provided in Chapter 1. For definitions of other terms refer to the Glossary.

10.1 Climate Summary

10.1.1 Current Climate

- Air temperatures in Palau show very little seasonal variation with less than 1°C difference between the warmest and coolest months.
- February, March and April are the driest months of the year in Koror, and the main wet season is from May to October.
- Rainfall is influenced by the West Pacific Monsoon, the Intertropical Convergence Zone and Palau's location within the Pacific Warm Pool region.
- Year-to-year variability in Palau's climate is strongly associated with El Niño-Southern Oscillation.
- Warming trends are evident in both annual and seasonal mean air temperatures at Koror for the period 1953–2009.
- Annual and seasonal rainfall trends for Koror for the period 1950–2009 are not statistically significant.
- The sea-level rise measured by satellite altimeters since 1993 is over 0.35 inches (9 mm) per year.
- Tropical cyclones (typhoons) are rare as Palau is south of the main typhoon zone. However, tropical storms and typhoons which pass to the north of Palau occasionally bring heavy rains and strong winds to the Palau Islands.

10.1.2 Future Climate

Over the course of the 21st century:

- Surface air temperature and sea-surface temperature are projected to continue to increase (*very high* confidence).
- Annual and seasonal mean rainfall is projected to increase (*moderate* confidence).
- The intensity and frequency of days of extreme heat are projected to increase (*very high* confidence).
- The intensity and frequency of days of extreme rainfall are projected to increase (*high* confidence).
- The incidence of drought is projected to decrease (*moderate* confidence).
- Tropical cyclone numbers are projected to decline in the tropical North Pacific Ocean basin (0–15ºN, 130ºE –180ºE) (*moderate* confidence).
- Ocean acidification is projected to continue (*very high* confidence).
- Mean sea-level rise is projected to continue (*very high* confidence).

10.2 Country Description

Located between 3°N–9°N and 131°E–135°E, Palau is a small country in the north-west tropical Pacific, 500 miles (800 km) east of the Philippines. There are over 500 islands in Palau most of which are small, uninhabited rock Islands. Total land area is 206 square miles (535 km^2) making Palau one of the smallest nations in the world (Palau's First National Communication under the UNFCCC, 2002).

Palau is divided into 16 states and the estimated population in 2010 was 20 518 (Palau Country Statistics, SOPAC, 2010). About 80% of its population live in Koror (both an island and state) (Office of Environmental Response and Coordination, 2002). Melekeok, on the bigger but less developed island of Babeldaob to the north, replaced Koror as the capital in October 2006.

The economy in Palau consists of tourism, subsistence agriculture and fishing and is relatively large when compared with other countries in Micronesia (Palau's Pacific Adaptations to Climate Change, 2010).

Figure 10.1: Palau

10.3 Data Availability

Palau has five operational meteorological observation stations. Multiple observations within a 24-hour period are taken at Koror and at the Palau International Airport. Climate observations are taken once a day at Kayangel, Nekken and Peleliu. Data are available for Koror (Figure 10.1) from 1948 for rainfall and 1953 for air temperature. Data from 1950 have been used. Koror data are homogeneous and more than 95% complete.

Monthly-averaged sea-level data are available from 1969 at Malakal-B (1969–present). Both satellite (from 1993) and in situ sea-level data (1950–2009; termed reconstructed sea level; Volume 1, Section 2.2.2.2) are available on a global 1° x 1° grid.

Long-term locally-monitored sea-surface temperature data are unavailable for Palau, so large-scale gridded sea-surface temperature datasets have been used (HadISST, HadSST2, ERSST and Kaplan Extended SST V2; Volume 1, Table 2.3).

10.4 Seasonal Cycles

Temperatures in Palau have very little seasonal variation. In Koror (Figure 10.2) the mean daily air temperature is about 82ºF (28°C) throughout the year and there is only a 1.5ºF (0.8°C) difference between the hottest and coolest month. The average relative humidity is 82%. Being on a small island surrounded by ocean, air temperatures in Koror are closely related to the sea-surface temperatures (Figure 10.2).

February, March and April are the driest months in Koror (Figure 10.2), and the main wet season is from May to October. The West Pacific Monsoon is usually most active and brings heavy rainfall between June and August. Average rainfall remains above 8 inches (200 mm) in all months of the year due to the Palau's location within the West Pacific Warm Pool and the year-long influence of the Intertropical Convergence Zone (ITCZ). Winds are generally moderate, and the north-easterly trades prevail from December through to March. During April, the frequency of trade winds decreases, and there is an increase in frequency of easterly winds. In May, the winds are predominantly from south-east to north-east.

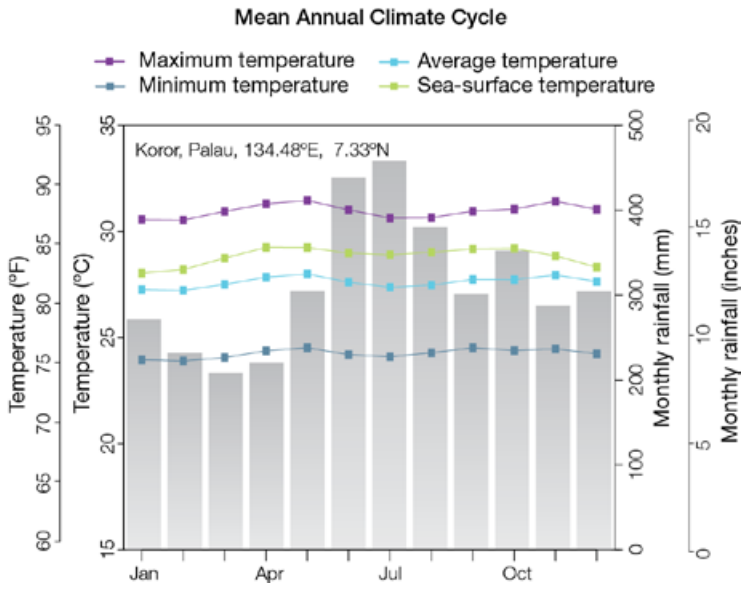

Figure 10.2: Mean annual cycle of rainfall (grey bars) and daily maximum, minimum and mean air temperatures at Koror, and local sea-surface temperatures derived from the HadISST dataset (Volume 1, Table 2.3).

10.5 Climate Variability

The interannual variability in rainfall at Koror is high and is mainly influenced by the El Niño-Southern Oscillation (ENSO). Generally, El Niño years are drier than average and La Niña years are wetter (Figure 10.4). A shortened wet season is usual for Koror during El Niño and prolonged wet season is normal during La Niña years. The dry season can extend to a six-month period with little rainfall during El Niño so the dry season rainfall amounts are much lower (see the correlation coefficients with ENSO indices in Table 10.1). This can lead to water rationing, as was the case during El Niño events in 1997/98 and the first half of 2010. During the El Niño event in 2002, however, the drought was not as severe and no water restrictions were required.

ENSO also influences air temperatures in Koror during the wet season (Table 10.1). In El Niño years wet season minimum air temperatures are usually above average while maximum air temperatures are below average.

ENSO Modoki events (Volume 1, Section 3.4.1) have similar impacts to canonical ENSO events, although the relationship is generally weaker for Modoki events (Table 10.1).

Table 10.1: Correlation coefficients between indices of key large-scale patterns of climate variability and minimum and maximum temperatures (Tmin and Tmax) and rainfall at Koror. Only correlation coefficients that are statistically significant at the 95% level are shown.

Climate feature/index		Wet season (May-October)			Dry season (November-April)		
		Tmin	Tmax	Rain	Tmin	Tmax	Rain
ENSO	Niño3.4	0.50	-0.28				-0.76
	Southern Oscillation Index	-0.38	0.41				0.70
Interdecadal Pacific Oscillation Index							
ENSO Modoki Index		0.36	-0.32				-0.41
Number of years of data		53	53	61	53	53	60

Training in *Pacific Climate Futures*, Palau National Weather Service

10.6 Observed Trends

10.6.1 Air Temperature

Warming trends are evident in both annual and seasonal mean air temperatures at Koror for the period 1953–2009 (Figure 10.3). Stronger mean air temperature trends are found in the dry season (November-April) when compared with the wet season (May-October) (Table 10.2).

10.6.2 Rainfall

Annual and seasonal rainfall trends for Koror for the period 1950–2009 are not statistically significant (Table 10.2 and Figure 10.4).

10.6.3 Extreme Events

Tropical cyclones (typhoons) are rare, as Palau is south of the main typhoon zone. However, tropical storms and typhoons which pass to the north of Palau occasionally bring heavy rains and strong winds to the Palau Islands. Typically, if a large typhoon or tropical storm passes between Guam and Yap (Federated States of Micronesia), a heavy swell is generated that may have sufficient strength to damage reefs.

10.6.4 Sea-Surface Temperature

Historical sea-surface temperature changes around Palau are consistent with the broad-scale sea-surface temperature changes for the PCCSP region. Water temperatures remained relatively constant from the 1950s to the late 1980s (although there is some disagreement between datasets). This was followed by a period of more rapid warming (approximately 0.23°F (0.13°C) per decade for 1970–present). Figure 10.6 shows the 1950–2000 sea-surface temperature changes (relative to a reference year of 1990) from three different large-scale sea-surface temperature gridded datasets (HadSST2, ERSST and Kaplan Extended SST V2; Volume 1, Table 2.3). At these regional scales, natural variability may play a large role in determining the sea-surface temperature making it difficult to identify any long-term trends.

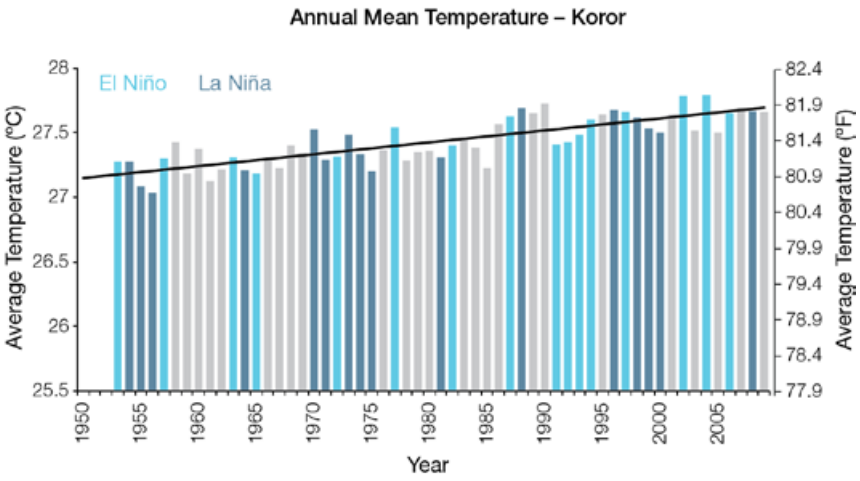

Figure 10.3: Annual mean air temperature at Koror. Light blue, dark blue and grey bars denote El Niño, La Niña and neutral years respectively.

Table 10.2: Annual and seasonal trends in maximum, minimum and mean air temperature (Tmax, Tmin and Tmean; 1953–2009) and rainfall (1950–2009) at Koror. Asterisks indicate significance at the 95% level. Persistence is taken into account in the assessment of significance as in Power and Kociuba (in press). The statistical significance of the air temperature trends is not assessed.

	Koror Tmax °F per 10 yrs (°C per 10 yrs)	Koror Tmin °F per 10 yrs (°C per 10 yrs)	Koror Tmean °F per 10 yrs (°C per 10 yrs)	Koror Rain inches per 10 yrs (mm per 10 yrs)
Annual	+0.19 (+0.11)	+0.14 (+0.08)	+0.17 (+0.09)	+0.21 (+5)
Wet season	+0.11 (+0.06)	+0.13 (+0.07)	+0.12 (+0.07)	-0.52 (-13)
Dry season	+0.29 (+0.16)	+0.16 (+0.09)	+0.22 (+0.12)	+0.87 (+22)

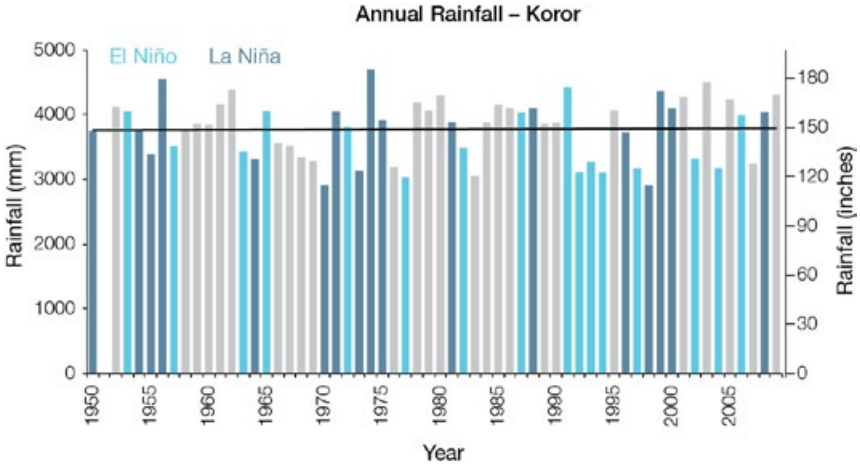

Figure 10.4: Annual rainfall for Koror. Light blue, dark blue and grey bars denote El Niño, La Niña and neutral years respectively.

10.6.5 Ocean Acidification

Based the large-scale distribution of coral reefs across the Pacific and the seawater chemistry, Guinotte et al. (2003) suggested that seawater aragonite saturation states above 4 were optimal for coral growth and for the development of healthy reef ecosystems, with values from 3.5 to 4 adequate for coral growth, and values between 3 and 3.5, marginal. Coral reef ecosystems were not found at seawater aragonite saturation states below 3 and these conditions were classified as extremely marginal for supporting coral growth.

In the Palau region, the aragonite saturation state has declined from about 4.5 in the late 18th century to an observed value of about 3.9 ± 0.1 by 2000.

10.6.6 Sea Level

Monthly averages of the historical tide gauge (since 1969), satellite (since 1993) and gridded sea-level (since 1950) data agree well after 1993 and indicate interannual variability in sea levels of about 14 inches (36 cm) (estimated 5–95% range) after removal of the seasonal cycle (Figure 10.9).

The sea-level rise near Palau measured by satellite altimeters (Figure 10.5) since 1993 is over 0.3 inches (9 mm) per year, larger than the global average of 0.125 ± 0.015 inches (3.2 ± 0.4 mm) per year. This rise is partly linked to a pattern related to climate variability from year to year and decade to decade (Figure 10.9).

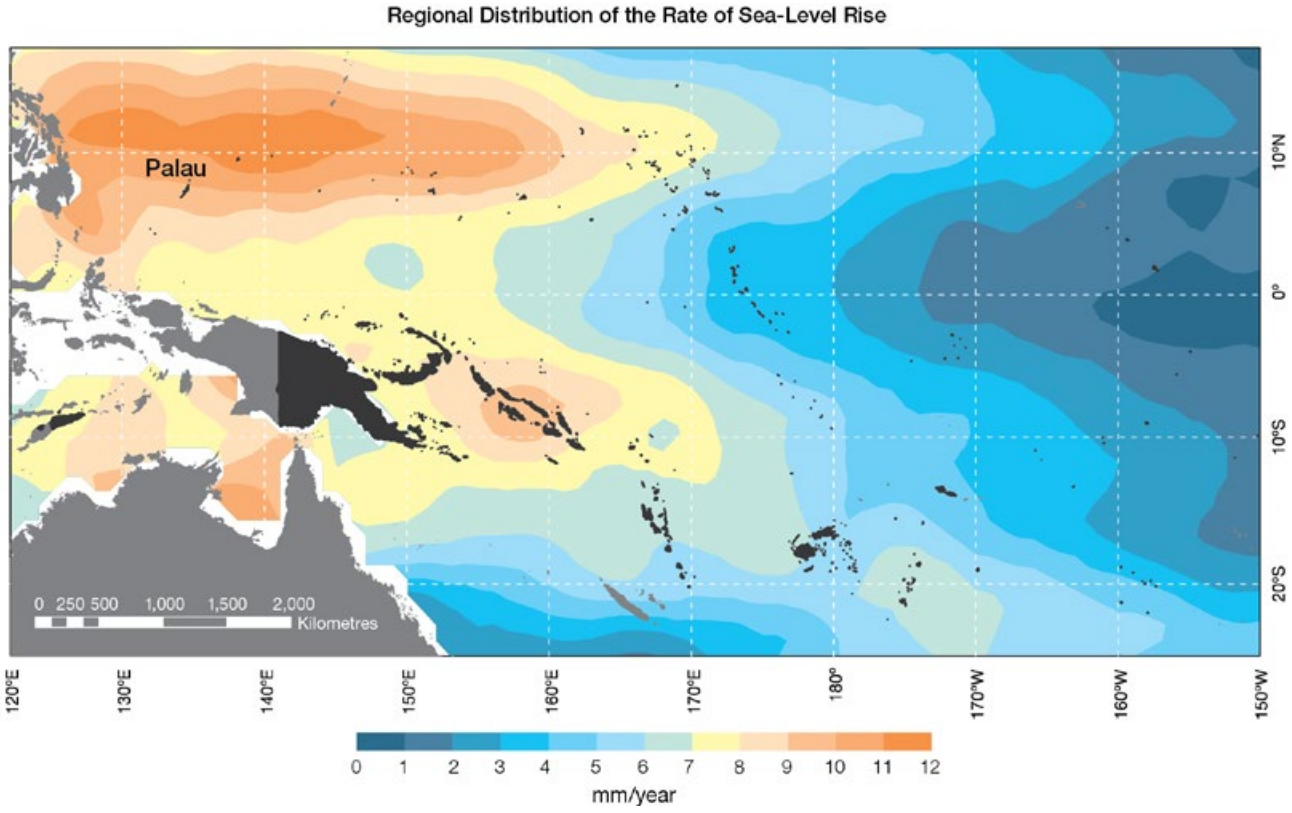

Figure 10.5: The regional distribution of the rate of sea-level rise measured by satellite altimeters from January 1993 to December 2010, with the location of Palau indicated. Further detail about the regional distribution of sea-level rise is provided in Volume 1, Section 3.6.3.2.

10.6.7 Extreme Sea-Level Events

The annual climatology of the highest daily sea levels has been evaluated from hourly measurements by tide gauges at Malakal Harbor, Palau (Figure 10.6). Highest tides tend to occur around the equinoxes, with the September peak the larger of the two. The average seasonal cycle shows little variation throughout the year. However, there is a strong ENSO influence with sea levels higher by over 0.3 ft (0.1 m) during La Niña years and the increase is most pronounced from July to January. The short-term components show little variation throughout the year and exhibit a small increase during La Niña years in January and February. The seasonal and tidal components combine to create a highest likelihood of extreme water levels from August through October. Five of the top 10 water levels recorded at Malakal cluster around the September maximum in tidal levels, indicating the strong influence of tides on extreme sea level occurrence, however, the remaining five are spread throughout the remainder of the year. Six of the 10 extreme events occurred during La Niña conditions, with the remaining four occurring during ENSO-neutral conditions, indicating the additional influence of ENSO on seasonal sea levels.

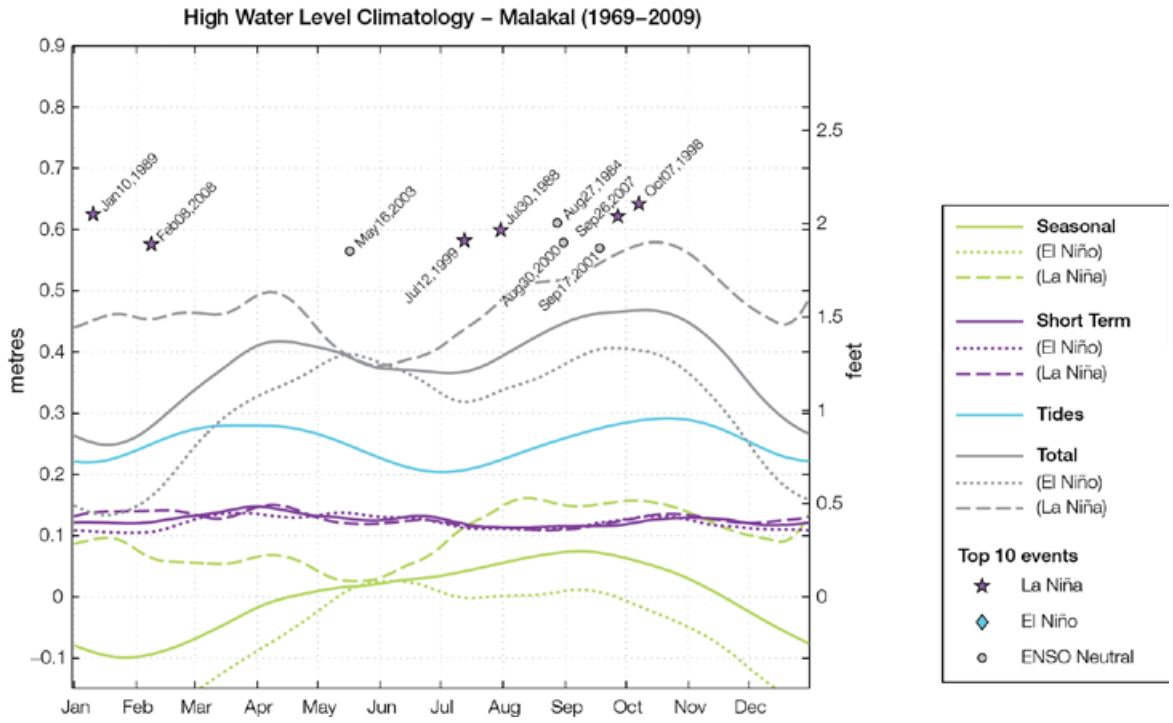

Figure 10.6: The annual cycle of high waters relative to Mean Higher High Water (MHHW) due to tides, short-term fluctuations (most likely associated with storms) and seasonal variations for Palau. The tides and short-term fluctuations are respectively the 95% exceedence of the astronomical high tides relative to MHHW and short-term sea level fluctuations. Components computed only for El Niño and La Niña years are shown by dotted and dashed lines, and grey lines are the sum of the tide, short-term and seasonal components. The 10 highest sea-level events in the record relative to MHHW are shown and coded to indicate the phase of ENSO at the time of the extreme event.

10.7 Climate Projections

Climate projections have been derived from up to 18 global climate models from the CMIP3 database, for up to three emissions scenarios (B1 (low), A1B (medium) and A2 (high)) and three 20-year periods (centred on 2030, 2055 and 2090, relative to 1990). These models were selected based on their ability to reproduce important features of the current climate (Volume 1, Section 5.2.3), so projections from each of the models are plausible representations of the future climate. This means there is not one single projected future for Palau, but rather a range of possible futures. The full range of these futures is discussed in the following sections.

These projections do not represent a value specific to any actual location, such as a town in Palau. Instead, they refer to an average change over the broad geographic region encompassing the islands of Palau and the surrounding ocean (Figure 1.1 shows the regional boundaries). Section 1.7 provides important information about understanding climate model projections.

10.7.1 Temperature

Surface air temperature and sea-surface temperature are projected to continue to increase over the course of the 21st century. There is *very high* confidence in this direction of change because:

- Warming is physically consistent with rising greenhouse gas concentrations.
- All CMIP3 models agree on this direction of change.

The majority of CMIP3 models simulate a slight increase (<1.8°F; <1°C) in annual and seasonal mean temperature by 2030, however by 2090 under the A2 (high) emissions scenario temperature increases of greater than 4.5°F (2.5°C) are simulated by almost all models (Table 10.3). Given the close relationship between surface air temperature and sea-surface temperature, a similar (or slightly weaker) rate of warming is projected for the surface ocean (Figure 10.7). There is *high* confidence in this range and distribution of possible futures because:

- There is generally close agreement between modelled and observed temperature trends over the past 50 years in the vicinity of Palau, although observational records are limited (Figure 10.7).

Interannual variability in surface air temperature and sea-surface temperature over Palau is strongly influenced by El Niño-Southern Oscillation (ENSO) in the current climate (Section 10.5). As there is no consistency in projections of future ENSO activity (Volume 1, Section 6.4.1) it is not possible to determine whether interannual variability in temperature will change in the future. However, ENSO is expected to continue to be an important source of variability for the region.

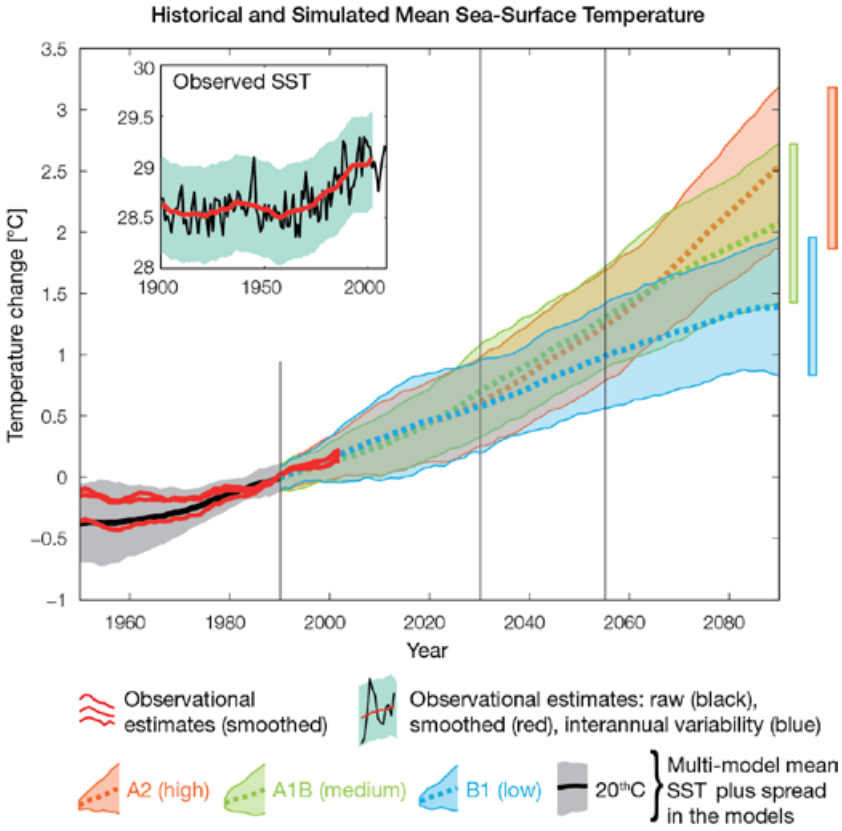

Figure 10.7: Historical climate (from 1950 onwards) and simulated historical and future climate for annual mean sea-surface temperature (SST) in the region surrounding Palau, for the CMIP3 models. Shading represents approximately 95% of the range of model projections (twice the inter-model standard deviation), while the solid lines represent the smoothed (20-year running average) multi-model mean temperature. Projections are calculated relative to the 1980–1999 period (which is why there is a decline in the inter-model standard deviation around 1990). Observational estimates in the main figure (red lines) are derived from the HadSST2, ERSST and Kaplan Extended SST V2 datasets (Volume 1, Section 2.2.2). Annual average (black) and 20-year running average (red) HadSST2 data is also shown inset.

10.7.2 Rainfall

Wet season (May-October), dry season (November-April) and annual average rainfall are projected to increase over the course of the 21st century. There is *moderate* confidence in this direction of change because:

- Physical arguments indicate that rainfall will increase in the equatorial Pacific in a warmer climate (IPCC, 2007; Volume 1, Section 6.4.3).
- Approximately half of the CMIP3 models agree on this direction of change by 2090.

The majority of CMIP3 models simulate little change (-5% to 5%) in rainfall by 2030, however by 2090 the models tend to be equally divided between an increase (>5%) and little change, with very few models simulating a decrease (<-5%) (Table 10.3). There is *moderate* confidence in this range and distribution of possible futures because:

- In simulations of the current climate, the CMIP3 models broadly capture the influence of the West Pacific Monsoon and Intertropical Convergence Zone on the rainfall in Palau (Volume 1, Sections 5.2.3.4 and 5.2.3.5), although most models produce monsoon westerly winds that do not extend far enough east into the Pacific basin.
- The CMIP3 models are unable to resolve many of the physical processes involved in producing rainfall. As a consequence, they do not simulate rainfall as well as other variables such as temperature (Volume 1, Chapter 5).

Interannual variability in rainfall over Palau is strongly influenced by ENSO in the current climate (Section 10.5). As there is no consistency in projections of future ENSO activity (Volume 1, Section 6.4.1), it is not possible to determine whether interannual variability in rainfall will change in the future.

10.7.3 Extremes

Temperature

The intensity and frequency of days of extreme heat are projected to increase over the course of the 21st century. There is *very high* confidence in this direction of change because:

- An increase in the intensity and frequency of days of extreme heat is physically consistent with rising greenhouse gas concentrations.
- All CMIP3 models agree on the direction of change for both intensity and frequency.

The majority of CMIP3 models simulate an increase of approximately 1.8°F (1°C) in the temperature experienced on the 1-in-20-year hot day by 2055 under the B1 (low) emissions scenario, with an increase of over 4.5°F (2.5°C) simulated by the majority of models by 2090 under the A2 (high) emissions scenario (Table 10.3). There is *low* confidence in this range and distribution of possible futures because:

- In simulations of the current climate, the CMIP3 models tend to underestimate the intensity and frequency of days of extreme heat (Volume 1, Section 5.2.4).
- Smaller increases in the frequency of days of extreme heat are projected by the CCAM 60 km simulations.

Rainfall

The intensity and frequency of days of extreme rainfall are projected to increase over the course of the 21st century. There is *high* confidence in this direction of change because:

- An increase in the frequency and intensity of extreme rainfall is consistent with larger-scale projections, based on the physical argument that the atmosphere is able to hold more water vapour in a warmer climate (Allen and Ingram, 2002; IPCC, 2007). It is also consistent with physical arguments that rainfall will increase in the deep tropical Pacific in a warmer climate (IPCC, 2007; Volume 1, Section 6.4.3).
- Almost all of the CMIP3 models agree on this direction of change for both intensity and frequency.

The majority of CMIP3 models simulate an increase of at least 0.4 inches (10 mm) in the amount of rain received on the 1-in-20-year wet day by 2055 under the B1 (low) emissions scenario, with an increase of at least 0.8 inches (20 mm) simulated by 2090 under the A2 (high) emissions scenario. The majority of models project that the current 1-in-20-year extreme rainfall event will occur, on average, two to three times per 20-year period by 2055 under the B1 (low) emissions scenario and four times per 20-year period by 2090 under the A2 (high) emissions scenario. There is *low* confidence in this range and distribution of possible futures because:

- In simulations of the current climate, the CMIP3 models tend to underestimate the intensity and frequency of extreme rainfall (Volume 1, Section 5.2.4).
- The CMIP3 models are unable to resolve many of the physical processes involved in producing extreme rainfall.

Drought

The incidence of drought is projected to decrease over the course of the 21st century. There is *moderate* confidence in this direction of change because:

- A decrease in drought is consistent with projections of increased rainfall (Section 10.7.2).
- The majority of models agree on this direction of change for most drought categories.

The majority of CMIP3 models project that mild drought will occur approximately seven to eight times every 20 years in 2030 under all emissions scenarios, decreasing to six to seven times by 2090. The frequency of moderate drought is projected to decrease from once to twice every 20 years in 2030, to once every 20 years in 2090 for all emissions scenarios, while the majority of CMIP3 models project that severe droughts

will occur less than once every 20 years across all time periods and scenarios. There is *low* confidence in this range and distribution of possible futures because:

- There is only moderate confidence in the range of rainfall projections (Section 10.7.2), which directly influences projections of future drought conditions.

Tropical Cyclones (Typhoons)

Tropical cyclone numbers are projected to decline in the tropical North Pacific Ocean basin (0–15ºS, 130ºE–180ºE) over the course of the 21st century. There is *moderate* confidence in this direction of change because:

- Many studies suggest a decline in tropical cyclone frequency globally (Knutson et al., 2010).
- Tropical cyclone numbers decline in the tropical North Pacific Ocean basin in the majority assessment techniques.

Based on the direct detection methodologies (Curvature Vorticity Parameter (CVP) and the CSIRO Direct Detection Scheme (CDD) described in Volume 1, Section 4.8.2), 80% of projections show no change or a decrease in tropical cyclone formation when applied to the CMIP3 climate models for which suitable output is available. When these techniques are applied to CCAM, 100% of projections show a decrease in tropical cyclone formation. In addition, the Genesis Potential Index (GPI) empirical technique suggests that conditions for tropical cyclone formation will become less favourable in the North Pacific Ocean basin, for the majority (70%) of analysed CMIP3 models. There is *moderate* confidence in this range and distribution of possible futures because:

- In simulations of the current climate, the CVP, CDD and GPI methods capture the frequency of tropical cyclone activity reasonably well (Volume 1, Section 5.4).

Consistent with this projected reduction in total cyclone numbers, five of the six 60 km CCAM simulations also show a decrease in the proportion of the most severe storms (those stronger than the current climate 90th percentile storm maximum wind speed). Most simulations project an increase in the proportion of storms occurring in the weaker categories. Associated with this is a reduction in cyclonic wind hazard.

10.7.4 Ocean Acidification

The acidification of the ocean will continue to increase over the course of the 21st century. There is *very high* confidence in this projection as the rate of ocean acidification is driven primarily by the increasing oceanic uptake of carbon dioxide, in response to rising atmospheric carbon dioxide concentrations.

Projections from all analysed CMIP3 models indicate that the annual maximum aragonite saturation state will reach values below 3.5 by about 2040 and continue to decline thereafter (Figure 10.8; Table 10.3). There is *moderate* confidence in this range and distribution of possible futures because the projections are based on climate models without an explicit representation of the carbon cycle and with relatively low resolution and known regional biases.

The impact of acidification change on the health of reef ecosystems is likely to be compounded by other stressors including coral bleaching, storm damage and fishing pressure.

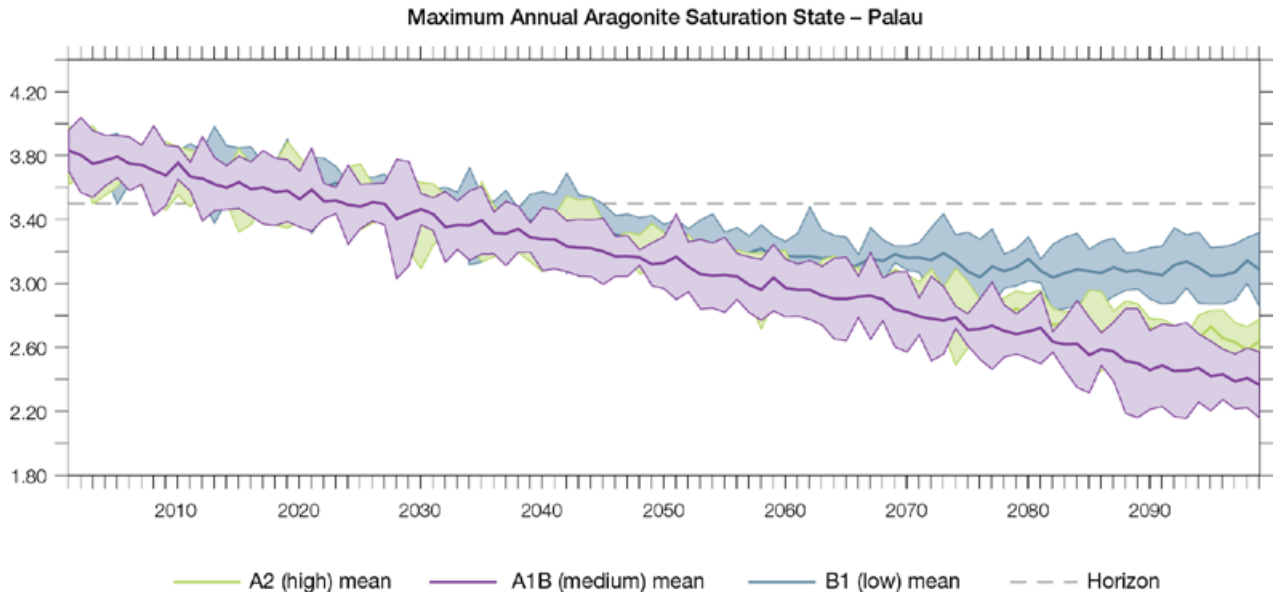

Figure 10.8: Multi-model projections, and their associated uncertainty (shaded area represents two standard deviations), of the maximum annual aragonite saturation state in the sea surface waters of the Palau region under the different emissions scenarios. The dashed black line represents an aragonite saturation state of 3.5.

10.7.5 Sea Level

Mean sea level is projected to continue to rise over the course of the 21st century. There is *very high* confidence in this direction of change because:

- Sea-level rise is a physically consistent response to increasing ocean and atmospheric temperatures, due to thermal expansion of the water and the melting of glaciers and ice caps.
- Projections arising from all CMIP3 models agree on this direction of change.

The CMIP3 models simulate a rise of between approximately 5–15 cm by 2030, with increases of 20–60 cm indicated by 2090 under the higher emissions scenarios (i.e. A2 (high), A1B (medium); Figure 10.9; Table 10.3). There is *moderate* confidence in this range and distribution of possible futures because:

- There is significant uncertainty surrounding ice-sheet contributions to sea-level rise and a rise larger than projected cannot be excluded (Meehl et al., 2007b). However, understanding of the processes is currently too limited to provide a best estimate or an upper bound (IPCC, 2007).
- Globally, since the early 1990s, sea level has been rising near the upper end of the these projections. During the 21st century, some studies (using semi-empirical models) project faster rates of sea-level rise.

Interannual variability of sea level will lead to periods of lower and higher regional sea levels. In the past, this interannual variability has been about 36 cm (5–95% range, after removal of the seasonal signal; dashed lines in Figure 10.9 (a)) and it is likely that a similar range will continue through the 21st century. In addition, winds and waves associated with weather phenomena will continue to lead to extreme sea-level events.

In addition to the regional variations in sea level associated with ocean and mass changes, there are ongoing changes in relative sea level associated with changes in surface loading over the last glacial cycle (glacial isostatic adjustment) and local tectonic motions. The glacial isostatic motions are relatively small for the PCCSP region.

10.7.6 Projections Summary

The projections presented in Section 10.7 are summarised in Table 10.3. For detailed information regarding the various uncertainties associated with the table values, refer to the preceding text in Sections 10.7 and 1.7, in addition to Chapters 5 and 6 in Volume 1. When interpreting the differences between projections for the B1 (low), A1B (medium) and A2 (high) emissions scenarios, it is also important to consider the emissions pathways associated with each scenario (Volume 1, Figure 4.1) and the fact that a slightly different subset of models was available for each (Volume 1, Appendix 1).

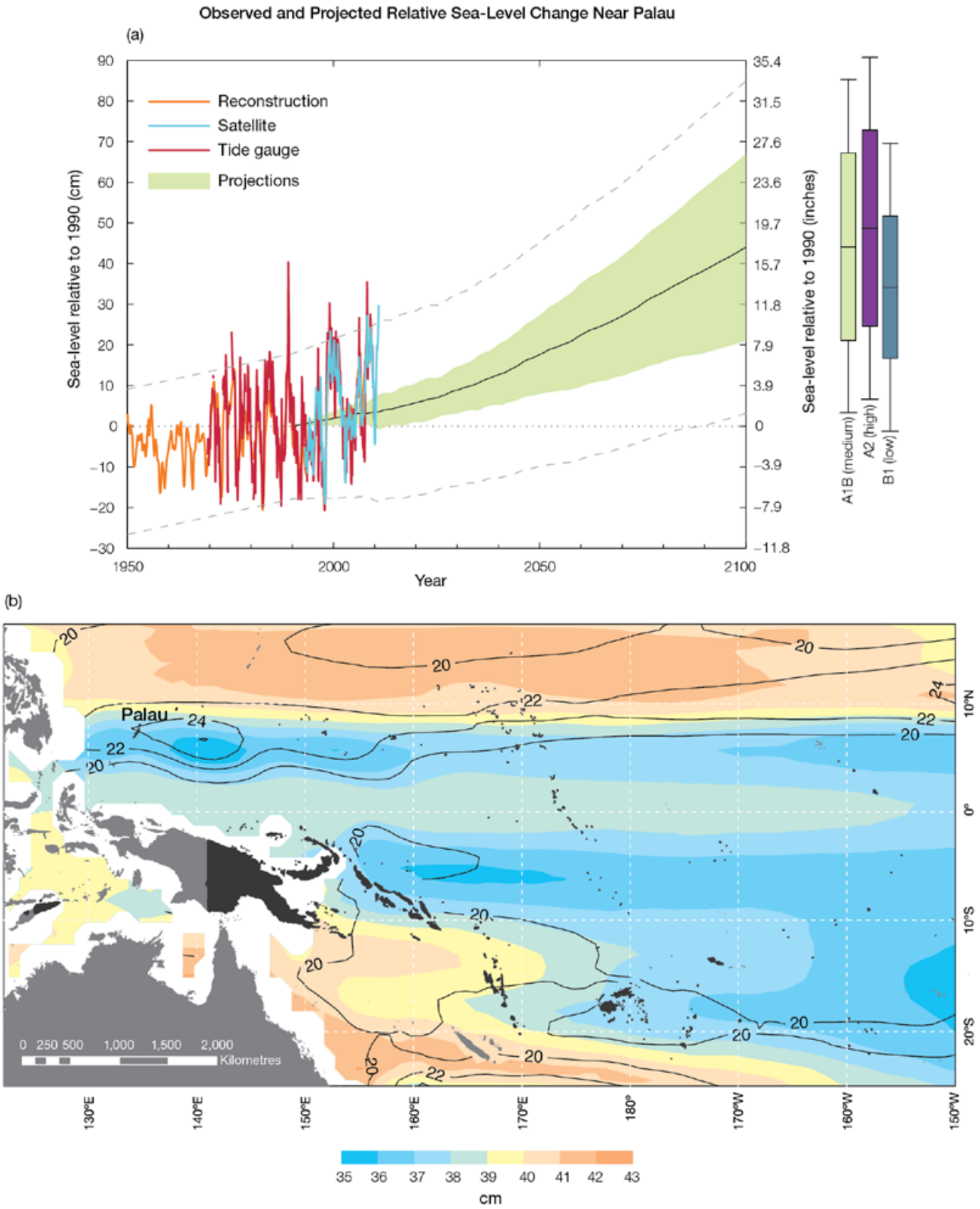

Figure 10.9: Observed and projected relative sea-level change near Palau. (a) The observed in situ relative sea-level records are indicated in red, with the satellite record (since 1993) in light blue. The gridded sea level at Palau (since 1950, from Church and White (in press)) is shown in orange. The projections for the A1B (medium) emissions scenario (5–95% uncertainty range) are shown by the green shaded region from 1990–2100. The range of projections for the B1 (low), A1B (medium), A2 (high) emissions scenarios by 2100 are also shown by the bars on the right. The dashed lines are an estimate of interannual variability in sea level (5–95% range about the long-term trends) and indicate that individual monthly averages of sea level can be above or below longer-term averages. (b) The projections (in cm) for the A1B (medium) emissions scenario in the Palau region for the average over 2081–2100 relative to 1981–2000 are indicated by the shading, with the estimated uncertainty in the projections indicated by the contours (in cm).

Table 10.3: Projected change in the annual and seasonal mean climate for Palau, under the B1 (low; blue), A1B (medium; green) and A2 (high; purple) emissions scenarios. Projections are given for three 20-year periods centred on 2030 (2020–2039), 2055 (2046–2065) and 2090 (2080–2099), relative to 1990 (1980–1999). Values represent the multi-model mean change ± twice the inter-model standard deviation (representing approximately 95% of the range of model projections), except for sea level where the estimated mean change and the 5–95% range are given (as they are derived directly from Intergovernmental Panel on Climate Change Fourth Assessment Report values). The confidence (Section 1.7.2) associated with the range and distribution of the projections is also given (indicated by the standard deviation and multi-model mean, respectively). See Volume 1, Appendix 1 for a complete listing of CMIP3 models used to derive these projections.

Variable	Season	2030	2055	2090	Confidence
Surface air temperature (°F)	Annual	+1.1 ± 0.7 +1.4 ± 0.7 +1.2 ± 0.5	+1.9 ± 0.8 +2.6 ± 0.9 +2.5 ± 0.8	+2.7 ± 1.2 +4.1 ± 1.5 +4.9 ± 1.3	High
Surface air temperature (°C)	Annual	+0.6 ± 0.4 +0.8 ± 0.4 +0.7 ± 0.3	+1.0 ± 0.4 +1.4 ± 0.5 +1.4 ± 0.4	+1.5 ± 0.7 +2.3 ± 0.8 +2.7 ± 0.7	High
Maximum temperature (°F)	1-in-20-year event	N/A	+1.6 ± 1.1 +2.5 ± 1.3 +2.5 ± 0.9	+2.3 ± 1.3 +3.8 ± 1.8 +4.9 ± 2.3	Low
Maximum temperature (°C)	1-in-20-year event	N/A	+0.9 ± 0.6 +1.4 ± 0.7 +1.4 ± 0.5	+1.3 ± 0.7 +2.1 ± 1.0 +2.7 ± 1.3	Low
Minimum temperature (°F)	1-in-20-year event	N/A	+2.2 ± 2.5 +2.7 ± 2.5 +2.5 ± 2.5	+2.9 ± 2.3 +3.8 ± 2.9 +4.1 ± 2.9	Low
Minimum temperature (°C)	1-in-20-year event	N/A	+1.2 ± 1.4 +1.5 ± 1.4 +1.4 ± 1.4	+1.6 ± 1.3 +2.1 ± 1.6 +2.3 ± 1.6	Low
Total rainfall (%)	Annual	0 ± 12 +2 ± 12 +1 ± 11	+3 ± 14 +4 ± 17 +2 ± 10	+5 ± 10 +8 ± 18 +6 ± 16	Moderate
Dry season rainfall (%)	November-April	0 ± 15 +3 ± 13 +1 ± 15	+3 ± 19 +4 ± 23 +2 ± 17	+5 ± 16 +7 ± 24 +4 ± 24	Moderate
Wet season rainfall (%)	May-October	0 ± 12 +2 ± 14 +1 ± 11	+3 ± 12 +5 ± 17 +3 ± 9	+5 ± 11 +9 ± 18 +8 ± 16	Moderate
Sea-surface temperature (°F)	Annual	+1.1 ± 0.7 +1.3 ± 0.7 +1.1 ± 0.7	+1.8 ± 0.7 +2.3 ± 0.7 +2.2 ± 0.7	+2.5 ± 1.1 +3.8 ± 1.1 +4.5 ± 1.3	High
Sea-surface temperature (°C)	Annual	+0.6 ± 0.4 +0.7 ± 0.4 +0.6 ± 0.4	+1.0 ± 0.4 +1.3 ± 0.4 +1.2 ± 0.4	+1.4 ± 0.6 +2.1 ± 0.6 +2.5 ± 0.7	High
Aragonite saturation state (Ωar)	Annual maximum	+3.5 ± 0.1 +3.4 ± 0.1 +3.4 ± 0.2	+3.2 ± 0.2 +3.0 ± 0.1 +3.0 ± 0.2	+3.0 ± 0.2 +2.6 ± 0.1 +2.5 ± 0.2	Moderate
Mean sea level (inches)	Annual	+3.1 (1.6–5.1) +3.5 (1.2–5.9) +3.5 (1.6–5.9)	+6.7 (3.1–10.2) +7.9 (3.5–12.2) +7.9 (4.3–11.4)	+11.8 (5.9–18.1) +15.0 (7.1–23.2) +16.1 (8.3–24.0)	Moderate
Mean sea level (cm)	Annual	+8 (4–13) +9 (3–15) +9 (4–15)	+17 (8–26) +20 (9–31) +20 (11–29)	+30 (15–46) +38 (18–59) +41 (21–61)	Moderate

*The MIROC3.2(medres) and MIROC3.2(hires) models were eliminated in calculating the rainfall projections, due to their inability to accurately simulate present-day activity of the West Pacific Monsoon and the Intertropical Convergence Zone, respectively (Volume 1, Section 5.5.1).